nanomaterials

MDPI

Article

Atomic-Scale Friction on Monovacancy-Defective Graphene and Single-Layer Molybdenum-Disulfide by Numerical Analysis

Haosheng Pang [1,†], Hongfa Wang [1,†], Minglin Li [1,2,*] and Chenghui Gao [1,*]

1 School of Mechanical Engineering and Automation, Fuzhou University, Fuzhou, Fujian 350002, China; m150210010@fzu.edu.cn (H.P.); hongfawang05@163.com (H.W.)
2 Fujian Key Laboratory of Medical Instrumentation and Pharmaceutical Technology, Fuzhou University, Fuzhou, Fujian 350002, China
* Correspondence: liminglin@fzu.edu.cn (M.L.); gch@fzu.edu.cn (C.G.)
† These authors contributed equally to this work.

Received: 6 December 2019; Accepted: 26 December 2019; Published: 2 January 2020

Abstract: Using numerical simulations, we study the atomic-scale frictional behaviors of monovacancy-defective graphene and single-layer molybdenum-disulfide ($SLMoS_2$) based on the classical Prandtl–Tomlinson (PT) model with a modified interaction potential considering the Schwoebel–Ehrlich barrier. Due to the presence of a monovacancy defect on the surface, the frictional forces were significantly enhanced. The effects of the PT model parameters on the frictional properties of monovacancy-defective graphene and $SLMoS_2$ were analyzed, and it showed that the spring constant of the pulling spring c_x is the most influential parameter on the stick–slip motion in the vicinity of the vacancy defect. Besides, monovacancy-defective $SLMoS_2$ is found to be more sensitive to the stick–slip motion at the vacancy defect site than monovacancy-defective graphene, which can be attributed to the complicated three-layer-sandwiched atomic structure of $SLMoS_2$. The result suggests that the soft tip with a small spring constant can be an ideal candidate for the observation of stick–slip behaviors of the monovacancy-defective surface. This study can fill the gap in atomic-scale friction experiments and molecular dynamics simulations of 2D materials with vacancy-related defects.

Keywords: numerical simulations; Prandtl–Tomlinson (PT) model; Schwoebel–Ehrlich barrier; monovacancy-defective graphene and single-layer molybdenum-disulfide ($SLMoS_2$); atomic-scale friction

1. Introduction

Atomic-scale friction has been at the forefront of scientific interest over the decades. Generally, the study on the friction at atomic-scale is significant because it can result in a fundamental understanding of how friction happens as well as to facilitate the development of nanomechanical components [1–3]. With the advent of tip-based microscopy techniques such as the lateral force microscopy (LFM) [4], the study on atomic-scale frictional processes became accessible to researchers, and the field of nano-tribology has been set up since then [5–8]. Through the detection of torsional deflections of a cantilever as the tip is dragged over a surface, LFM can be applied to characterize the topographic and tribological features of nanomaterials [9,10]. The first observation of atomic-scale frictional phenomenon was reported by Mate et al. for a tungsten tip sliding on a graphite surface [4]. By means of a LFM, they found the atomic-scale stick–slip motion of the lateral force with the periodicity of graphite's honeycomb structure. Since then, the origin and variation of atomic-scale friction have been thoroughly explored by tribologists.

As one of the most remarkable discoveries in nano-tribology, the atomic-scale stick–slip phenomenon appears in the time domain as a series of saw-tooth signals, and its period usually corresponds to the unit cell of the surface potential [11,12]. This observation can be theoretically reproduced within classical mechanics by using the Prandtl–Tomlinson (PT) model, which describes the movement of a point-like tip connected to a support by a harmonic spring in constant-force mode of an idealized LFM. As the support moves at a constant speed, the tip is dragged by the spring to slide over a whole surface, while at the same time, feeling the force from a corrugated tip–surface interaction potential featuring atomic periodicity [13–16]. The stick–slip instability occurs when the tip moves through the regions where the curvature of the tip–surface interaction potential exceeds the elastic constant of the pulling spring. Otherwise, such instabilities completely vanish, and the tip exhibits a continuous, low-dissipative motion, commonly known as superlubricity [17].

Atomically-thin laminar two-dimensional (2D) materials, such as graphene and single-layer molybdenum-disulfide ($SLMoS_2$), are ideal candidates suited for atomic-scale frictional studies because these materials are air-stable, chemically inert [18], and can be easily cleaved to yield atomically flat surfaces with regular crystal structures [19]. However, the vacancy defects, known as the most commonly reported defects in graphene [20,21] and $SLMoS_2$ [22,23], are inevitable during the production process and can result in considerable changes in surface morphology. So far, most experimental, theoretical, and simulation studies on the atomic-scale friction of graphene and $SLMoS_2$ have focused on atomically flat surfaces [24–28]; nevertheless, these simplified idealizations cannot reflect the topography and frictional properties of many practical surfaces such as vacancy-defective surfaces. Molecular dynamics (MD) simulations have indicated that the frictional forces of defective graphene were significantly increased in the vicinity of vacancy point defects compared to that of the perfect graphene [29,30]. In the literature [29], Sun et al. thought the atomic friction of graphene with vacancy defects was similar to the sliding at an atomic-scale surface step and attributed the sharp variations in frictional forces to additional activation barriers (commonly referred to as the Schwoebel–Ehrlich barrier [31,32]) caused by the reduction of the atomic coordination at the vacancy defects. However, the sliding velocity of the tip in the above MD simulations was set to 2.5 m/s for [29] and 14.8 m/s for [30], respectively, which is much faster than that of typical experimental LFM set-ups (at the order of 10 nm/s [9]). Besides, the other parameters of the classical PT model, such as the effective masse of the system, the spring constant of the pulling spring, and the damping of the system, cannot be quantitatively adjusted in the MD simulation method or deduced from LFM experiments. Up to now, the effects of the PT model parameters on the atomic-scale frictional behaviors of the monovacancy-defective surface remain unclear, which hinders our understanding of the underlying mechanisms for atomic-scale frictional behaviors of defective 2D materials. As a supplement to the MD simulation and LFM experiments, the numerical approach is an efficient tool to obtain the theoretical solution of the PT model, recover the observed characteristics from the actual experiments and MD simulations, predict the results under conditions that cannot be tested experimentally and solved by MD simulations, and has been shown to accurately describe the frictional properties at atomic-scale surface steps [33,34].

In this work, we employ a novel numerical simulation method to explore the atomic-scale frictional properties of the monovacancy-defective graphene and $SLMoS_2$. A modified interaction potential considering the Schwoebel–Ehrlich barrier is developed for the tip-defective surface interaction potential of the PT model. To study the mechanisms that control the frictional characteristics of the graphene and $SLMoS_2$ with vacancy defects, we changed the effective masse of the system, the damping of the system, the sliding velocity of the tip, and the spring constant of the pulling spring to examine how the atomic-scale frictional behaviors depend on these variables. Ours is the first study revealing the influences of the classical PT model parameters on the atomic-scale frictional properties of a monovacancy-defective surface, and this work can make up for the deficiency of the LFM experiments and MD simulations when studying the atomic-scale frictional behaviors of 2D materials with vacancy-related defects.

2. Simulation Model and Method

Graphene consists of an isotropic hexagonal honeycomb lattice of carbon atoms. $SLMoS_2$ consists of a 2D hexagonal honeycomb lattice where the Mo layer is covalently sandwiched between the bottom S layer and the top S layer. The vertical distance between two S layers of $SLMoS_2$ is approximately 3.24 Å. The atomistic models of monovacancy-defective graphene and $SLMoS_2$ are achieved by constructing a defect-free monolayer film first and then introducing the monovacancy defect in the center of the surface/top layer, as shown in the inserts in Figure 1a,b. In the adopted Cartesian coordinate system, the X-axis is set along the zigzag (ZZ) direction, the Y-axis along the armchair (AC) direction, and the Z-axis normal to the graphene and $SLMoS_2$. The sliding was applied by moving the tip along the zigzag (ZZ) on the center line of the monovacancy-defective graphene and $SLMoS_2$. The areas of the graphene and $SLMoS_2$ film were 76.26×62.48 Å^2 and 166.23×142.59 Å^2 in the X–Y plane, respectively. The single-atom tip was generated for the atomic-scale friction according to the PT model, which consisted of a single carbon atom and was set as a rigid body in order to avoid the mass loss caused by the tip wear during the atomic-scale friction process. The constant-force mode is applied in the model and the loading force on the tip is kept at 2.5 nN. The schematic diagrams of the atomic-scale friction of monovacancy-defective graphene and $SLMoS_2$ are shown in Figure 1a,b, respectively.

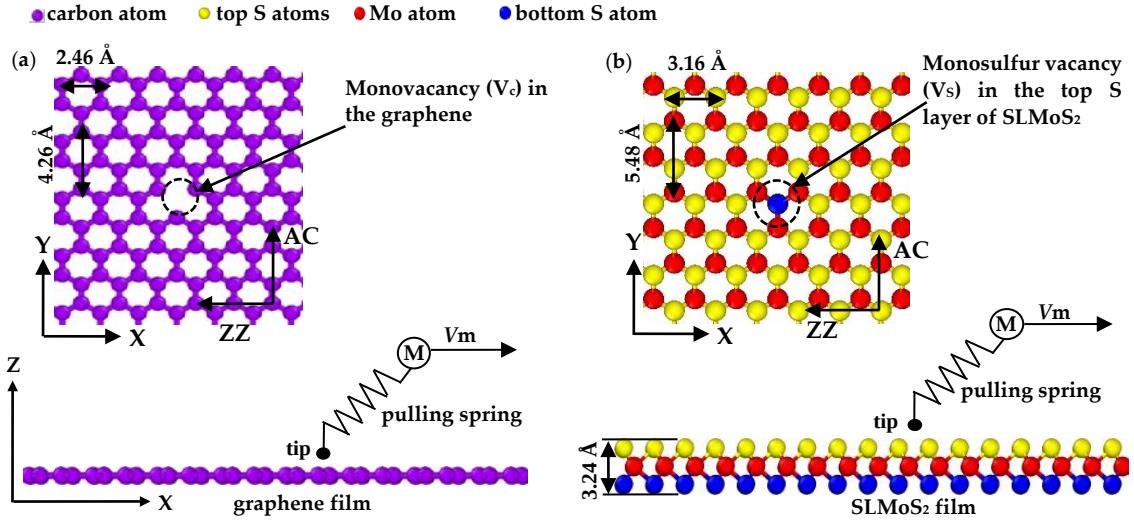

Figure 1. (**a**) The schematic diagram of the atomic-scale: the frictional interaction between a single-atom tip and the graphene with the monovacancy (Vc). (**b**) The schematic diagram of the atomic-scale: the frictional interaction between a single-atom tip and the $SLMoS_2$ with the monosulfur vacancy (Vs) in the top S layers. The tip is connected via a pulling spring with the elasticity of C to the body M and is moved along the X direction at a constant velocity of V_m.

In the atomic-scale friction process, stick–slip behaviors can be explained by the classical PT model, which simplifies the single-asperity friction into one point-mass (tip) pulled along a corrugated potential by a driving support (spring) [16]. The classical PT model is shown as follows:

$$\begin{aligned} m_x\ddot{x}_t &= c_x(x_M - x_t) - \frac{\partial V_{\text{int}}(x_t,y_t)}{\partial x_t} - \gamma_x\dot{x}_t \\ m_y\ddot{y}_t &= c_y(y_M - y_t) - \frac{\partial V_{\text{int}}(x_t,y_t)}{\partial y_t} - \gamma_x\dot{y}_t \end{aligned} \quad (1)$$

where c_x and c_y represent the spring constants of the pulling spring, m_x and m_y represent the effective masses of the system, x_t and y_t represent the actual positions of the tip, $x_M = y_M = V_m t$ represent the equilibrium positions of the tip without potential, V_m represents the sliding velocity of the tip, V_{int} (x_t, y_t) represents the tip–surface interaction potential, γ_x and γ_y represent the damping of the system. The frictional forces $F_x = c_x$ ($x_M - x_t$) and $F_y = c_y$ ($y_M - y_t$) of the PT model are composed of a dissipative part and a conservative part, which are given by the damping term and the tip–surface interaction

potential, respectively [15]. Theoretically, the degree of freedom for the atomic motions is high in 2D systems where the non-adiabatic motion is avoided [28]. In the PT model, the sweeping of the tip can be regarded as adiabatic.

The tip–surface interaction potential of the classical PT model in Equation (1) is governed by the corrugated potential V_{int} (x_t, y_t), which can be described as

$$V_{\text{int}}(x_t, y_t) = V_0 \cos\left(\frac{2\pi}{a_x} x_t\right) \cos\left(\frac{2\pi}{a_y} y_t\right) \tag{2}$$

where V_0 represents the initial value of tip-sample interaction, a_x and a_y represent the sample's lattice constants in the ZZ and AC orientation, respectively. In the ZZ orientation, a_x is 2.46 and 3.16 Å for graphene and $SLMoS_2$, respectively.

In order to quantify the tip–surface interaction potential, the Lennard–Jones (LJ) potential V_{LJ}, which has been used to accurately describe the frictional properties at atomic-scale steps [33,34], is taken into consideration as the tip–surface potential in the case of the single-atom tip crossing the monovacancy defects of graphene and $SLMoS_2$. The V_{LJ} can be described as follows:

$$V_{\text{LJ}} = \sum\nolimits_{i=1}^{N} E_0 \left((r_0/r_i)^{12} - 2(r_0/r_i)^6 \right) \tag{3}$$

where r_i represents the distance between the ith surface atom and the tip, r_0 and E_0 represent the equilibrium distance and the binding energy, respectively.

In the presence of the vacancy defects, the surface state is similar to that of the atomic-scale surface steps. According to previous LFM studies on the monovacancy-defective graphene [29,30] and the stepped surfaces [34–38], there is the Schwoebel–Ehrlich barrier existing in the vicinity of the vacancy defect, and hence the long-range interactions V_{long} are varying, which means a second contribution to the tip–surface interaction potential should be considered. A modified interaction potential V_{total} containing the periodic interaction V_{int} (x_t, y_t) between the tip and surface as well as the sharply increasing potential barrier at the vacancy defect site simulating the long-range interaction potential V_{long} is constructed to reflect the tip–surface interaction of the defective graphene and $SLMoS_2$ with monovacancy defects, which is shown as follows:

$$V_{\text{total}} = V_{\text{int}}(x_t, y_t) + V_{\text{long}} \tag{4}$$

The long-range interaction potential V_{long} can be described by the model [33,37,38] based on the approximate low-load analytical form of the Schwoebel–Ehrlich barrier in the vicinity of the atomic-scale surface step. The V_{long} is shown as follows:

$$V_{\text{long}}(x) = E\left[-\text{erf}\left(\frac{x}{b_1} - d\right) + \text{erf}\left(\frac{x-c}{b_2}\right)\right] \tag{5}$$

where E represents a constant of the order of an electronvolt, b_1 represents the effective barrier width at the vacancy defect site, b_2, c, and d are the constants representing a recovery of the potential away from the vacancy defect.

In order to obtain the numerical description of the frictional force F_x in the PT model, we develop the modified interaction potential V_{total} by fitting the LJ potential curve and set it as the approximate tip–surface interaction potential of the monovacancy-defective graphene and $SLMoS_2$. Relevant parameters for the LJ potential V_{LJ} and the long-range interaction V_{long} are shown in Tables S1 and S2 in the supporting materials, respectively. The simulations of the atomic-scale frictional behaviors in our work are performed by using the software Mathematica (Wolfram Research, Champaign, IL, USA, version 12).

3. Results and Discussions

We first calculate the tip–surface interaction potential by LJ potential (V_{LJ}) and then develop the modified interaction potential (V_{total}) through fitting the LJ potential (V_{LJ}). By introducing the potential V_{tota} into Equation (1), we can calculate the path of the tip on the sample surface and obtain the frictional forces. Finally, we discuss the effects of the parameters (the effective mass of the system m, damping of the system γ, sliding velocity V_m, and spring constant of the pulling spring c) of the classical PT model on the frictional force and the stick-slip behaviors of monovacancy-defective graphene and $SLMoS_2$.

Figure 2a,b shows the tip–surface potential P_t versus the sliding distance D curves when the tip moves over the vacancy defect at the surface of the defective graphene and $SLMoS_2$, respectively. The corresponding frictional force F_x versus the sliding distance D curves are shown in Figure 2c,d, respectively. The typical parameters of LFM experiments [15,28,39] are set as follows: $m_x = m_y = 10^{-8}$ kg, $c_x = c_y = 10$ N/m, $V_0 = 1.0$ eV, and $V_{\mathrm{m}} = 40$ nm/s. The damping of the system can be obtained with $\gamma_x = \gamma_y = 2\ (c_x\ m_x)^{1/2} \approx 10^{-3}$ N·s/m. Owing to the presence of the monovacancy defect, the changes in the tip–surface potential and frictional force of the monovacancy-defective graphene and $SLMoS_2$ can be clearly observed. There are the large positive tip–surface potential and frictional force occurring when the tip approaches the vacancy, indicating the attraction from the vacancy. After passing the vacancy, the tip feels a large attractive force from the vacancy again. The enhanced frictional force in the vicinity of the vacancy defect is in agreement with that in the previous works about the monovacancy-defective graphene [29,30], and the sharp variations in tip–surface potentials and frictional forces can be attributed to the Schwoebel–Ehrlich barriers [31,32], which have been already observed in the friction at the atomic-scale surface steps of graphene [34–36,38] and MoS_2 [37].

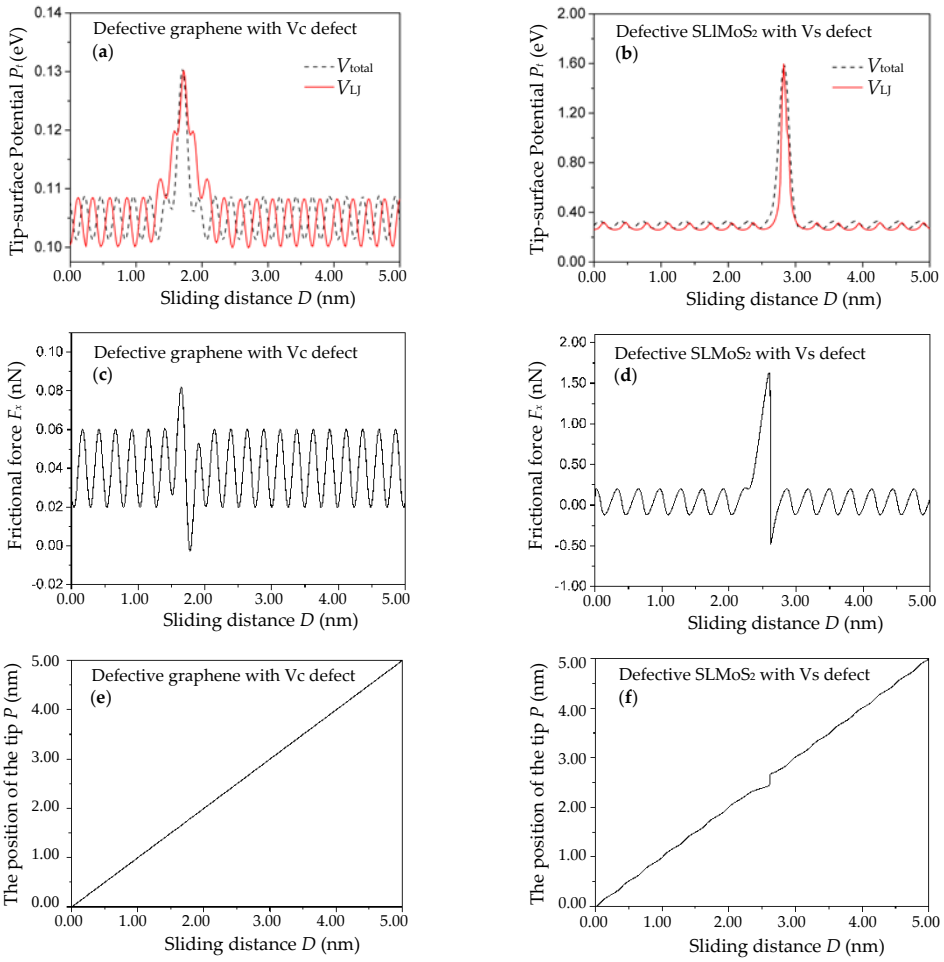

Figure 2. The tip-surface potential *Pt* vs. scanning distance *D* curves (**a**,**b**), the frictional force F_x vs. the sliding distance *D* curves (**c**,**d**), and the position of the single-atom tip *P* vs. the sliding distance *D* curves (**e**,**f**) of the monovacancy-defective graphene and $SLMoS_2$. The solid red curves and the dashed black curves in (**a**,**b**) were obtained by calculating the LJ potential (V_{LJ}) and by fitting the LJ potential (V_{LJ}) via the modified interaction potential (V_{total}), respectively.

In order to explore the stick–slip motions during the frictional process of the monovacancy-defective graphene and $SLMoS_2$, we plot the position of the single-atom tip versus the sliding distance curves, as illustrated in Figure 2e,f. It indicates that the stick–slip motion is absent for the friction of the monovacancy-defective graphene, while the obvious stick–slip motion appears in the vicinity of vacancy defect of monovacancy-defective $SLMoS_2$. It can be attributed to the difference in the curvature of the tip–surface interaction V'' (or the critical elastic constant c_x) at the vacancy defect site of defective graphene and $SLMoS_2$ ($V''_{carbon} = 0.91$ for the monovacancy-defective graphene and $V''_{SLMoS2} = 17.18$ for the monovacancy-defective $SLMoS_2$) because the stick–slip phenomenon occurs on condition that the elastic constant c_x of the pulling spring ($c_x = 10$ N/m, $c_x > V''_{carbon}$, and $c_x < V''_{SLMoS2}$) should be less than or equal to the curvature of the tip–surface interaction potential V'' [17,34]. Besides, although there is no stick–slip motion for the monovacancy-defective graphene, the single-atom tip does undergo periodical acceleration–deceleration motion without a full stick, which is similar to the stick–slip motion, and in accord with previous studies of defective graphene [30].

3.1. Variation of the Effective Masses m_x of the System

The relations of the frictional force F_x vs. the sliding distance *D* for four effective masses m_x of the system (namely, $m_x = 10^{-10}$, 5×10^{-9}, 3×10^{-8}, and 12×10^{-8} kg) are shown in Figure 3a,b.

The c_x, V_m, and γ_x are set to 10 N/m, 40 nm/s, and 10^{-3} N·s/m, respectively. It is seen that all the F_x-D curves of the monovacancy-defective graphene are almost the same, as shown in Figure 3a. For the monovacancy-defective $SLMoS_2$, however, the amplitude of the minimum frictional force $F_{x\min}$ increases with m_x (namely, the amplitude of F_{xmin} is 0.465, 0.468, 0.605, and 1.040 nN for $m_x = 10^{-10}$, 5×10^{-9}, 3×10^{-8}, and 12×10^{-8} kg, respectively), and the other frictional forces including the maximum frictional force $F_{x\max}$ and the periodic frictional forces (namely, the frictional forces except for that in the vicinity of the vacancy defect) remain basically unchanged, as shown in Figure 3b.

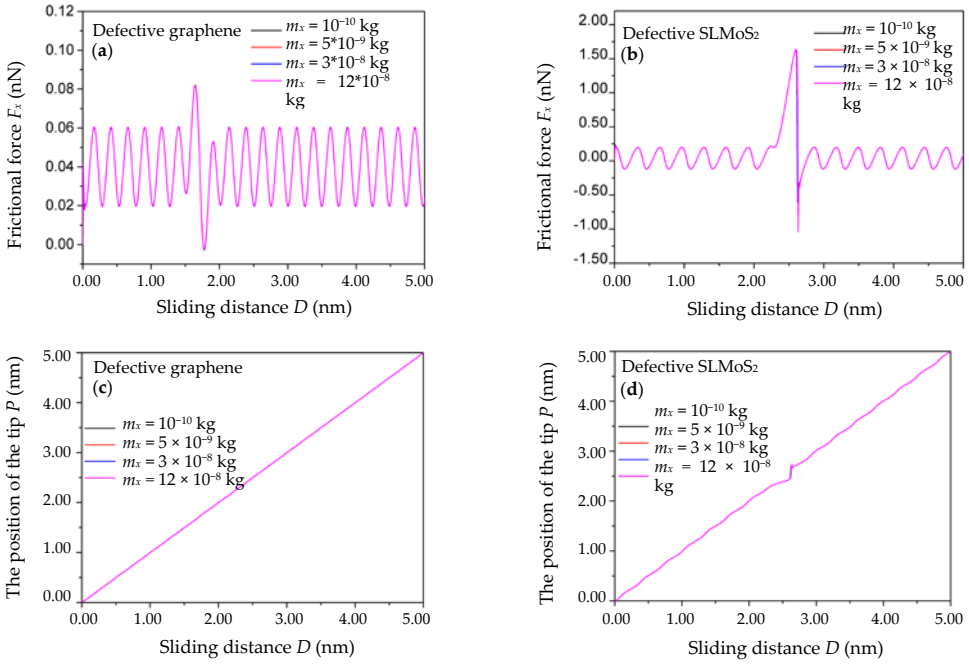

Figure 3. The frictional force F_x vs. the sliding distance D curves of the monovacancy-defective graphene (**a**) and $SLMoS_2$ (**b**) with different effective masses m_x of the system. The position of the single-atom tip P vs. the scanning distance D curves of the monovacancy-defective graphene (**c**) and $SLMoS_2$ (**d**) with different effective masses m_x of the system. The curves in Figure 3 look like a single curve, but they are the overlap of multiple curves, and the displayed curves are the pink curves.

The relations of the position of the single-atom tip P vs. the sliding distance D for the above four effective masses m_x of the system are shown in Figure 3c,d. It can be seen that there is virtually no change in the P vs. D curves of the monovacancy-defective graphene and $SLMoS_2$ with different m_x, which means the stick–slip motion in the vicinity of the vacancy defect is nearly independent of the effective masses m_x of the system.

3.2. Variation of the Damping γ_x of the System

The relations of the frictional force F_x vs. the sliding distance D for four different dampings γ_x of the system (namely, $\gamma_x = 8 \times 10^{-5}$, 4×10^{-4}, 2×10^{-3}, and 10^{-2} N·s/m) are shown in Figure 4a,b. The c_x, V_m, and m_x are set to 10 N/m, 40 nm/s, and 10^{-8} kg, respectively. The results show that the frictional forces F_x of the monovacancy-defective graphene and $SLMoS_2$ increase with the damping γ_x. It can be explained by Equation (1) that the frictional force $F_x = c_x\,(x_M - x_t) = m_x\ddot{x}_t + \partial V_{\text{int}}(x_t, y_t)/\partial x + \gamma_x\dot{x}_t$ is positively correlated with the damping γ_x, which is in agreement with the definition of the frictional force in the PT model [15]. However, the amplitudes of the frictional forces including the enhanced frictional forces in the vicinity of the vacancy defect and the periodic frictional forces of the monovacancy-defective graphene and $SLMoS_2$ increase with decreasing γ_x, as shown in Supplementary Figure S1a,b. This negative correlation between the amplitude of the frictional force and the damping γ_x is in accord

with the physical meaning of the damping term in the PT model, namely, the term considering the mechanisms of the energy dissipation in atomic-scale friction [15,16].

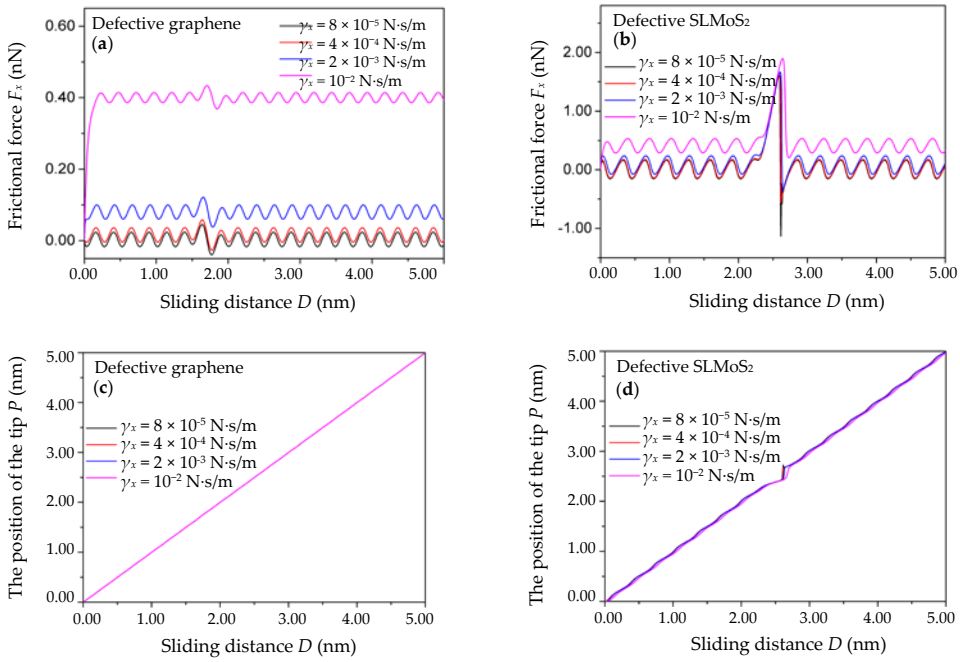

Figure 4. The frictional force F_x vs. the sliding distance D curves of the monovacancy-defective graphene (**a**) and $SLMoS_2$ (**b**) with different dampings γ_x of the system. The position of the single-atom tip P vs. the scanning distance D curves of the monovacancy-defective graphene (**c**) and $SLMoS_2$ (**d**) with different dampings γ_x of the system. The curves in Figure 4 look like a single curve, but they are the overlap of multiple curves, and the displayed curves are the pink curves.

The relations of the position of the single-atom tip P vs. the sliding distance D for the above four dampings γ_x of the system are shown in Figure 4c,d. The results show that the P vs. D curves of the monovacancy-defective graphene with different γ_x are coincident, and this trend is similar to that of the monovacancy-defective $SLMoS_2$ except for a little shift in the stick–slip regime at the defect position for the case of $\gamma_x = 10^{-2}$ N·s/m. It indicates that the damping γ_x of the system has little effect on the stick–slip motions in the vicinity of the vacancy defect.

3.3. Variation of the Sliding Velocity V_m

Figure 5a,b shows the relations of the frictional force F_x versus the sliding distance for five different sliding velocities V_m (namely, V_m = 2, 15, 60, and 150 nm/s). The γ_x, c_x, and m_x are set to 10^{-3} N·s/m, 10 N/m, and 10^{-8} kg, respectively. It is seen that the frictional forces of the monovacancy-defective graphene and $SLMoS_2$ increase with the V_m. The result can be explained by Equation (1) that the atomic-scale frictional force $F_x = c_x\,(x_M - x_\mathrm{t}) = c_x\,(V_\mathrm{m}t - x_\mathrm{t})$ [15,34] is positively correlated with the sliding velocity V_m, which has been demonstrated in previous work [40]. Besides, the amplitudes of the frictional forces including the enhanced frictional forces in the vicinity of the vacancy defect and the periodic frictional forces of the monovacancy-defective graphene and $SLMoS_2$ almost keep constant at different sliding velocities V_m.

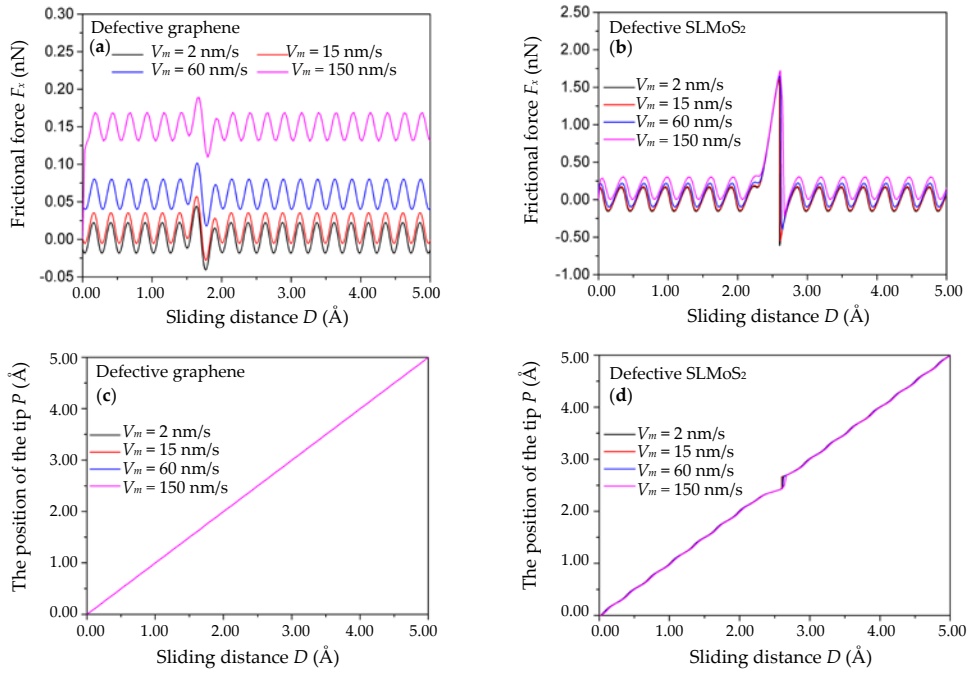

Figure 5. The frictional force F_x vs. the sliding distance D curves of the monovacancy-defective graphene (**a**) and $SLMoS_2$ (**b**) with different sliding velocities V_m. The position of the single-atom tip P vs. the scanning distance D curves of the monovacancy-defective graphene (**c**) and $SLMoS_2$ (**d**) with different sliding velocities V_m. The curves in Figure 5 look like a single curve, but they are the overlap of multiple curves, and the displayed curves are the pink curves.

The relations of the position of the single-atom tip P vs. the sliding distance D for the above four sliding velocities V_m are shown in Figure 5c,d. Similar to the trends of m_x and γ_x, the variations in the P vs. D curves of the monovacancy-defective graphene and $SLMoS_2$ with different V_m are extremely small and can be neglected, which indicates that the stick–slip motion in the vicinity of the vacancy defect is approximately independent of the sliding velocity V_m. The result seems to contradict previous studies suggesting that stick–slip motions can also be suppressed or even ruined by thermally activated jumps when the tip scans at a low velocity [41,42]. Nevertheless, this is because the temperature was not considered for the classical PT model in this work, and hence the resulting thermally activated fluctuations of the friction behaviors were not observed. We expect the effect of the temperature on the atomic-scale frictional properties of defective 2D materials to be systematically studied in future works.

3.4. Variation of the Spring Constants c_x of the Pulling Spring

Due to the great difference in the critical spring constants c_x (the curvature of the tip–surface interaction potential) of the monovacancy-defective graphene and $SLMoS_2$ in this work (the critical c_x is 0.91 and 17.18 N/m for the monovacancy-defective graphene and $SLMoS_2$, respectively, as calculated in the beginning of Section 3), it is reasonable to set three different c_x which are based on their respective critical values c_x and separated by a amplitude of 5 times. Specifically, the small spring constants c_x, the critical spring constants c_x, and the larger spring constants c_x of the monovacancy-defective graphene are set to 0.18, 0.91, and 4.55 N/m, respectively. The small spring constants c_x, the critical spring constants c_x, and the larger spring constants c_x of the monovacancy-defective $SLMoS_2$ are set to 3.44, 17.18, and 85.9 N/m, respectively. Figure 6a,b show the relations of the frictional force F_x versus the sliding distance for the three different spring constants c_x of the pulling spring. The γ_x, V_m, and m_x are set to 10^{-3} N·s/m, 40 nm/s, and 10^{-8} kg, respectively. It is seen that the amplitudes of the frictional forces of the monovacancy-defective graphene and $SLMoS_2$ increase with the spring constants c. However, the details of the observed variations in the frictional forces of two materials

are distinctly different. For the monovacancy-defective graphene, all the frictional forces including the enhanced frictional forces in the vicinity of the vacancy defect and the periodic frictional forces are positively correlated with the spring constants c_x. For the monovacancy-defective $SLMoS_2$, the maximum frictional force $F_{x\max}$ and the periodic frictional forces almost keep constant at different c_x while the amplitude of the minimum frictional force $F_{x\min}$ in the vicinity of vacancy point defects increases with the c_x.

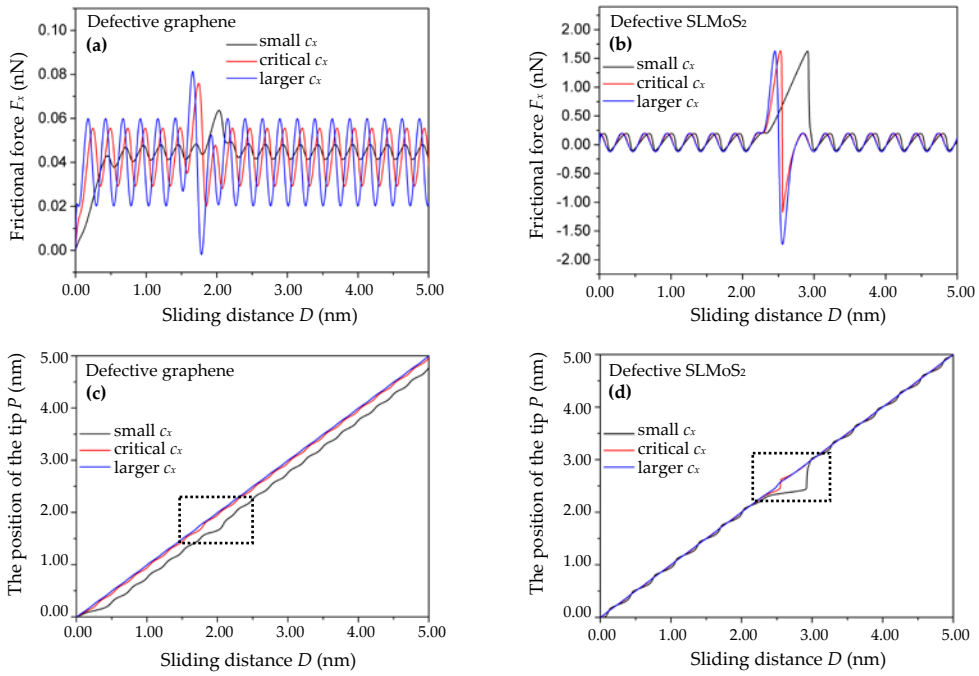

Figure 6. The frictional force F_x vs. the sliding distance D curves of the monovacancy-defective graphene (**a**) and $SLMoS_2$ (**b**) with different spring constants c_x of the pulling spring. The position of the single-atom tip P vs. the scanning distance D curves of the monovacancy-defective graphene (**c**) and $SLMoS_2$ (**d**) with different c_x. The small, critical, and larger c_x of the monovacancy-defective graphene in Figure 6a is 0.18, 0.91, and 4.55 N/m, respectively. The small, critical, and larger c_x of the monovacancy-defective $SLMoS_2$ in Figure 6b is 3.44, 17.18, and 85.9 N/m, respectively.

The relations of the position of the single-atom tip P vs. the sliding distance D for the above three spring constants c_x are shown in Figure 6c,d. It is observed that when the c_x of the monovacancy-defective graphene and $SLMoS_2$ are less than or equal to the critical value, the stick–slip behaviors occur and become more obvious as the spring constants c_x decrease (the black and red wavy lines in Figure 6c,d). Otherwise, the stick–slip behaviors disappear completely (the blue lines in Figure 6c,d). The results are in agreement with previous studies [15,17,34,43]. In addition, it is noted that the stick–slip behaviors in the vicinity of the vacancy defect of the monovacancy-defective $SLMoS_2$ are much more obvious than that of the monovacancy-defective graphene when their respective spring constants c_x are equal to or a fifth of the critical c_x (see the dotted boxes in Figure 6c,d). It indicates that it is more sensitive to the stick–slip motion at the vacancy defect site for the monovacancy-defective $SLMoS_2$ than that for the monovacancy-defective graphene, which can be due to the more complicated three-layer-sandwiched atomic structure of $SLMoS_2$. It is worth noting that $SLMoS_2$ [22] can be charged, which may influence the stick–slip motions around the vacancy defect. However, the interaction between the LFM tip and the $SLMoS_2$ with the charged state of the vacancy defect remains unclear so far, and we expect this issue will be deeply studied in future works. Besides, the influence of the chirality on the atomic-scale friction of monovacancy-defective 2D graphene and $SLMoS_2$ is also explored, and the results suggest that the variation trends of the stick–slip behaviors and the frictional forces along the AC orientation are similar to that along the ZZ orientation, as shown in Supplementary

Figures S2 and S3. Compared with the other parameters of the classical PT model (the effective masse of the system m_x, damping of the system γ_x, and sliding velocity V_m), the spring constant of the pulling spring c_x has the most remarkable impact on the stick–slip motion in the vicinity of the vacancy defect, which suggests that the soft tip with small spring constant can be suitable for the observation of the stick–slip motions in the atomic-scale friction experiments of the monovacancy-defective 2D materials. Otherwise, the stiff tip with larger spring constant can be suitable for the observation of the low-dissipative motions or the superlubricity phenomena in the atomic-scale friction experiments of the monovacancy-defective 2D materials.

4. Conclusions

In this work, we employed a numerical simulation method to explore the atomic-scale friction of monovacancy-defective 2D graphene and SLMoS_2 based on a classical PT model with a modified interaction potential considering the Schwoebel–Ehrlich barrier. It was found that the frictional forces are significantly enhanced due to the presence of a monovacancy defect on the surface. The effects of the PT model parameters (the effective masse of the system m_x, damping of the system γ_x, sliding velocity V_m, and spring constant of the pulling spring c_x) on the frictional properties of monovacancy-defective graphene and SLMoS_2 were analyzed. It revealed that the spring constant of the pulling spring c_x has the most remarkable impact on the stick–slip motion in the vicinity of the vacancy defect compared with other parameters. In addition, it is more sensitive to the stick–slip motion at the vacancy defect site for the monovacancy-defective SLMoS_2 than that for the monovacancy-defective graphene, which can be due to the complicated three-layer-sandwiched atomic structure of SLMoS_2. This study suggests that a soft tip with small spring constant can be an ideal candicate for the LFM experiment of stick–slip behaviors of the monovacancy-defective surface, and it can provide valuable complementary information for atomic-scale friction experiments and MD simulations of 2D materials with vacancy-related defects.

Supplementary Materials: The following are available online at http://www.mdpi.com/2079-4991/10/1/87/s1, Figure S1: The amplitudes of the maximum frictional forces F_{xmax} and the periodic frictional forces F_{xp} of the monovacancy-defective graphene and SLMoS_2 with different dampings γ_x of the system; Figure S2: The tip-surface potential Pt vs scanning distance D curves for sliding paths along AC orientation of the monovacancy-defective graphene and SLMoS_2; The position of the single-atom tip P vs the scanning distance D curves for sliding paths along AC orientation of the monovacancy-defective graphene and SLMoS_2 with different effective mass of the system m_x, damping of the system γ_x, sliding velocity V_m and spring constant of the pulling spring c_x; Figure S3: The frictional force F_x vs the sliding distance D curves for sliding paths along AC orientation of the monovacancy-defective graphene and SLMoS_2 with different effective mass of the system m_x, damping of the system γ_x, sliding velocity V_m and spring constant of the pulling spring c_x; Table S1: The parameters for the LJ potential V_LJ; Table S2: The parameters for the long-range interaction V_long of Figure 2a,b.

Author Contributions: Conceptualization, H.P., H.W. and M.L.; methodology, H.W.; software, H.W.; validation, H.P., H.W., M.L. and C.G.; formal analysis, H.P. and H.W.; investigation, H.P. and H.W.; resources, H.P. and H.W.; data curation, H.W.; writing—original draft preparation, H.P. and H.W.; writing—review and editing, H.P. and H.W.; visualization, H.P. and H.W.; supervision, M.L.; project administration, C.G.; funding acquisition, C.G., please turn to the CRediT taxonomy for the term explanation. Authorship must be limited to those who have contributed substantially to the work reported. All authors have read and agreed to the published version of the manuscript.

Funding: This research was funded by the National Natural Science Foundation of China (Grant Nos. 50903017, 51175085, and 51875106) and Natural Science Foundation of Fujian Province (Grant No. 2018J01509). Check carefully that the details given are accurate and use the standard spelling of funding agency names at https://search.crossref.org/funding, any errors may affect your future funding.

Acknowledgments: The authors are grateful for the National Natural Science Foundation of China (Grant Nos. 50903017, 51175085, and 51875106), Natural Science Foundation of Fujian Province (Grant No. 2018J01509) and the Fujian Provincial Collaborative Innovation Center for High-End Equipment Manufacturing. The authors are also grateful for the insightful discussions and continuous support from Ren Zhiying (Fuzhou University), Ye Kongqiang, Chen Zhiying and Lai Lianfeng (Ningde Normal University). Haosheng Pang and Hongfa Wang contributed equally to this work.

Conflicts of Interest: The authors declare no conflict of interest.

References

1. Manini, N.; Mistura, G.; Paolicelli, G.; Tosatti, E.; Vanossi, A. Current trends in the physics of nanoscale friction. *Adv. Phys.* **2017**, *2*, 569–590. [CrossRef]
2. Ye, F.; Lee, J.; Feng, P.X. Atomic layer MoS2-graphene van der Waals heterostructure nanomechanical resonators. *Nanoscale* **2017**, *9*, 18208. [CrossRef] [PubMed]
3. Dong, Y.; Li, Q.; Martini, A. Molecular dynamics simulation of atomic friction: A review and guide. *J. Vac. Sci. Technol. A* **2013**, *31*, 030801. [CrossRef]
4. Mate, C.M.; Mcclelland, G.M.; Erlandsson, R.; Chiang, S. Atomic-scale friction of a tungsten tip on a graphite surface. *Phys. Rev. Lett.* **1987**, *59*, 1942. [CrossRef]
5. Cui, Z.; Xie, G.; Feng, H.; Wang, W.; Wei, W. Atomic-scale Friction of Black Phosphorus: Effect of Thickness and Anisotropic Behavior. *Adv. Mater. Interfaces* **2017**, *4*, 1700998. [CrossRef]
6. Ouyang, W.; Wijn, A.S.D.; Urbakh, M. Atomic-scale sliding friction on contaminated surfaces. *Nanoscale* **2018**, *10*, 6375–6381. [CrossRef]
7. Li, S.; Li, Q.; Carpick, R.W.; Gumbsch, P.; Liu, X.Z.; Ding, X.; Sun, J.; Ju, L. The evolving quality of frictional contact with graphene. *Nature* **2016**, *539*, 541–545. [CrossRef]
8. Zeng, X.; Peng, Y.; Liu, L.; Lang, H.; Cao, X. Dependence of the friction strengthening of graphene on velocity. *Nanoscale* **2018**, *10*, 1855–1864. [CrossRef]
9. Zhang, S.; Ma, T.B.; Ali, E.; Li, Q. Tribology of two-dimensional materials: From mechanisms to modulating strategies. *Mater. Today* **2018**, *26*, 67–86. [CrossRef]
10. Lei, G.; Chen, X.; Yuan, M.; Yu, Y.; Qiao, L. Origin of moiré superlattice scale lateral force modulation of graphene on transition metal substrate. *Nanoscale* **2018**, *10*, 10576–10583.
11. Liu, Z.; Wang, W.; Liu, L. Comparative study on friction force pattern anisotropy of graphite. *Appl. Surf. Sci.* **2015**, *332*, 473–479. [CrossRef]
12. Tian, K.; Gosvami, N.N.; Goldsby, D.L.; Carpick, R.W. Stick-Slip Instabilities for Interfacial Chemical Bond-Induced Friction at the Nanoscale. *J. Phys. Chem. B* **2017**, *122*, 991–999. [CrossRef] [PubMed]
13. Jagla, E.A. The Prandtl-Tomlinson model of friction with stochastic driving. *J. Stat. Mech- Theory E* **2018**, *1*, 013401. [CrossRef]
14. Schwarz, U.D.; Hölscher, H. Exploring and explaining friction with the Prandtl-Tomlinson model. *ACS Nano* **2016**, *10*, 38–41. [CrossRef] [PubMed]
15. Hölscher, H.; Schwarz, U.D.; Wiesendanger, R. Modelling of the scan process in lateral force microscopy. *Surf. Sci.* **1997**, *375*, 395–402. [CrossRef]
16. Wang, Z.J.; Ma, T.B.; Hu, Y.Z.; Xu, L.; Wang, H. Energy dissipation of atomic-scale friction based on one-dimensional Prandtl-Tomlinson model. *Friction* **2015**, *3*, 170–182. [CrossRef]
17. Socoliuc, A.; Bennewitz, R.; Gnecco, E.; Meyer, E. Transition from stick-slip to continuous sliding in atomic friction: Entering a new regime of ultralow friction. *Phys. Rev. Lett.* **2004**, *92*, 134301. [CrossRef]
18. Chu, X.S.; Yousaf, A.; Li, D.O.; Tang, A.A.; Debnath, A.; Ma, D.; Green, A.A.; Santos, E.J.G.; Wang, Q.H. Direct covalent chemical functionalization of unmodified two-dimensional molybdenum disulfide. *Chem. Mater.* **2018**, *30*, 2112–2128. [CrossRef]
19. Guo, Y.; Liu, C.; Yin, Q.; Wei, C.; Lin, S.; Hoffman, T.B.; Zhao, Y.; Edgar, J.H.; Chen, Q.; Lau, S.P. Distinctive in-plane cleavage behaviors of two-dimensional layered materials. *ACS Nano* **2016**, *10*, 8980–8988. [CrossRef]
20. Rajasekaran, G.; Narayanan, P.; Parashar, A. Effect of point and line defects on mechanical and thermal properties of graphene: A Review. *Crit. Rev. Solid State* **2015**, *41*, 47–71. [CrossRef]
21. Chu, L.; Shi, J.; de Souza Cursi, E. Vibration analysis of vacancy defected graphene sheets by monte carlo based finite element method. *Nanomaterials* **2018**, *8*, 489. [CrossRef] [PubMed]
22. Zhou, W.; Zou, X.; Najmaei, S.; Liu, Z.; Shi, Y.; Kong, J.; Lou, J.; Ajayan, P.M.; Yakobson, B.I.; Idrobo, J.C. Intrinsic structural defects in monolayer molybdenum disulfide. *Nano Lett.* **2013**, *13*, 2615–2622. [CrossRef]
23. Wang, W.; Yang, C.; Bai, L.; Li, M.; Li, W. First-principles study on the structural and electronic properties of monolayer MoS_2 with S-vacancy under uniaxial tensile strain. *Nanomaterials* **2018**, *8*, 74. [CrossRef] [PubMed]
24. Pang, H.; Li, M.; Gao, C.; Lai, L.; Zhuo, W. Characterization of frictional properties of single-layer molybdenum-disulfide film based on a coupling of tip radius and tip–sample distance by molecular dynamics simulations. *Nanomaterials* **2018**, *8*, 387. [CrossRef]

25. Ky, D.L.C.; Khac, B.C.T.; Le, C.T.; Yong, S.K.; Chung, K.H. Friction characteristics of mechanically exfoliated and CVD-grown single-layer MoS_2. *Friction* **2018**, *6*, 395–406. [CrossRef]
26. Lee, C.; Li, Q.; Kalb, W.; Liu, X.Z.; Berger, H.; Carpick, R.W.; Hone, J. Frictional characteristics of atomically thin sheets. *Science* **2010**, *328*, 76–80. [CrossRef]
27. Ye, Z.; Egberts, P.; Han, G.H.; Johnson, A.T.; Carpick, R.W.; Martini, A. Load-dependent friction hysteresis on graphene. *ACS Nano* **2016**, *10*, 5161–5168. [CrossRef]
28. Li, M.; Shi, J.; Liu, L.; Yu, P.; Xi, N.; Wang, Y. Experimental study and modeling of atomic-scale friction in zigzag and armchair lattice orientations of MoS_2. *Sci. Technol. Adv. Mat.* **2016**, *17*, 189–199. [CrossRef]
29. Sun, X.Y.; Wu, R.N.; Xia, R.; Chu, X.H.; Xu, Y.J. Effects of Stone-Wales and vacancy defects in atomic-scale friction on defective graphite. *Appl. Phys. Lett.* **2014**, *104*, 2605. [CrossRef]
30. Liu, P.; Zhang, Y.W. A theoretical analysis of frictional and defect characteristics of graphene probed by a capped single-walled carbon nanotube. *Carbon* **2011**, *49*, 3687–3697. [CrossRef]
31. Schwoebel, R.L. Step motion on crystal surfaces. *J. Cryst. Growth* **1969**, *40*, 614–618. [CrossRef]
32. Ehrlich, G. Atomic displacements in one- and two-dimensional diffusion. *J. Chem. Phys.* **1966**, *44*, 1050–1055. [CrossRef]
33. Pascal, S.; Enrico, G.; Franciszek, K.; Janusz, B.; Lukasz, W.; Jerzy, K.; Marek, S.; Ernst, M. Atomic-scale friction on stepped surfaces of ionic crystals. *Phys. Rev. Lett.* **2011**, *106*, 186104.
34. Hendrik, H.; Daniel, E.; Schwarz, U.D. Friction at atomic-scale surface steps: Experiment and theory. *Phys. Rev. Lett.* **2009**, *101*, 246105.
35. Vasić, B.; Matković, A.; Gajić, R.; Stanković, I. Wear properties of graphene edges probed by atomic force microscopy based lateral manipulation. *Carbon* **2016**, *107*, 723–732. [CrossRef]
36. Chen, Z.; Khajeh, A.; Martini, A.; Kim, S.H. Chemical and physical origins of friction on surfaces with atomic steps. *Sci. Adv.* **2019**, *5*, 8. [CrossRef]
37. Boland, M.J.; Nasseri, M.; Hunley, D.P.; Ansary, A.; Strachan, D.R. Striped nanoscale friction and edge rigidity of MoS 2 layers. *RSC Adv.* **2015**, *5*, 92165–92173. [CrossRef]
38. Hunley, D.P.; Flynn, T.J.; Dodson, T.; Sundararajan, A.; Boland, M.J.; Strachan, D.R. Friction, adhesion, and elasticity of grahene edges. *Phys. Rev. B* **2013**, *87*, 8004. [CrossRef]
39. Fujisawa, S.; Kishi, E.; Sugawara, Y.; Morita, S. Atomic-scale friction observed with a two-dimensional frictional-force microscope. *Phys. Rev. B* **1995**, *51*, 7849–7857. [CrossRef]
40. Fusco, C.; Fasolino, A. Velocity dependence of atomic-scale friction: A comparative study of the one-and two-dimensional Tomlinson model. *Phys. Rev. B* **2005**, *71*, 045413. [CrossRef]
41. Krylov, S.Y.; Jinesh, K.B.; Valk, H.; Dienwiebel, M.; Frenken, J.W.M. Thermally induced suppression of friction at the atomic scale. *Phys. Rev. E* **2005**, *71*, 325–326. [CrossRef] [PubMed]
42. Krylov, S.Y.; Frenken, J.W.M. Atomic-scale friction experiments reconsidered in the light of rapid contact dynamics. *Phys. Rev. B* **2009**, *80*, 235435. [CrossRef]
43. Hölscher, H.; Schirmeisen, A.; Schwarz, U.D. Principles of atomic friction: From sticking atoms to superlubric sliding. *Philos. T. R. Soc. A* **2008**, *366*, 1383–1404. [CrossRef] [PubMed]